

Multi-Factor Spatio-Temporal Prediction based on Graph Decomposition Learning

Jiahao Ji, Jingyuan Wang, Yu Mou, and Cheng Long

Abstract—Spatio-temporal (ST) prediction is an important and widely used technique in data mining and analytics, especially for ST data in urban systems such as transportation data. In practice, the ST data generation process is usually affected by a mixture of multiple latent factors related to natural phenomena or human socioeconomic activities. Different factors generally affect some spatial areas but not all of them. However, existing ST prediction methods usually do not refine the impacts of different factors, but directly model the entangled impacts of multiple factors. This can increase the modeling difficulty of ST data and hurt the model interpretability at the same time. To this end, we propose a multi-factor spatio-temporal prediction task that predicts the evolution of the partial ST data under different factors separately and then combines them to produce a final overall prediction. We make two contributions to this task: an effective theoretical solution and a portable instantiation framework. Specifically, we first propose a theoretical solution called decomposed prediction strategy and prove its effectiveness from the perspective of information entropy theory. On top of that, we instantiate a novel model-agnostic framework, named spatio-temporal graph decomposition learning (STGDL), for multi-factor ST prediction. The framework consists of two main components: an automatic graph decomposition module that decomposes the original graph structure inherent in ST data into several subgraphs corresponding to different factors, and a decomposed learning network that learns the partial ST data on each subgraph separately and integrates them for the final prediction. The framework is theoretically guaranteed to reduce the prediction error and enhance the interpretability of predicted ST data. We conduct extensive experiments on four real-world ST datasets of two types of graphs, i.e., grid graph and network graph. Results show that our portable framework significantly reduces prediction errors of various ST models by 9.41% on average (35.36% at most). Furthermore, a case study reveals the interpretability potential of our framework as well as its predictions. Our code is at <https://github.com/bigscity/STGDL>.

Index Terms—Spatio-Temporal Data Mining, Decomposed Prediction Strategy, Graph Decomposition, Traffic Flow Prediction

1 INTRODUCTION

WITH the ubiquitous use of GPS-enabled mobile devices and sensors, a huge volume of spatio-temporal (ST) data is emerging from a variety of domains, *e.g.*, urban transportation, meteorology, and public health. Through ST prediction techniques [1], [2], [3], [4], the ST data can support a growing number of applications ranging from individual smart mobility [5] to public safety management [6]. For example, ST traffic prediction, which aims to accurately forecast future traffic conditions from past traffic observations, can promote environmentally friendly commuting through bike-sharing initiatives [7], [8], and enhance traffic efficiency through congestion management [9], [10].

Existing studies on ST data usually take a temporal and spatial perspective. The temporal perspective describes the data evolution trends over time, which covers patterns of closeness, periodicity, and trend [11], [12]. Researchers apply the recurrent neural networks (*e.g.*, LSTM) [13], [14], temporal convolutional networks [15], [16], or attention mechanism [17] to encode the temporal features of traffic series. On the other hand, the spatial perspective mainly describes the relations of different spatial regions or sensors in the study area [18], [19]. All the relations are mixed

together to form a global graph structure. Main efforts deploy graph neural networks for holistic spatial dependency modeling [4], [20], [21], or attention mechanism for spatial information aggregation across the whole graph [3], [16].

Despite their notable successes, the existing methods generally adopt a holistic scheme, *i.e.*, characterizing ST data on the original graph structure as a whole. They ignore the nuances among partial ST data affected by different latent factors. Each factor may only affect relevant graph nodes and relations rather than the whole. Taking traffic ST data as an example, the formation of traffic flow typically follows the human mobility law in real-world socioeconomic interactions [22]. It is driven by many complex latent factors, such as commuting, entertainment, business, *etc.* Each of them focuses on different urban regions and forms different traffic flows [23], [24], [25], [26]. The complex and entangled relations among multiple latent factors bring an urge for decoupling these factors in ST data prediction. This remains unexplored by the existing works. As a result, the predicted ST data contains a mixture of entangled factors, inevitably harming interpretability and causing difficulties in thoroughly understanding the evolution of ST data.

In this paper, we propose a *multi-factor spatio-temporal prediction* task to tackle the multi-factor issue. The task aims to forecast the ST data evolution of multiple latent factors separately and then integrate all partial results for the final ST prediction. We design a novel Spatio-Temporal Graph Decomposition Learning framework (STGDL) capable of the multi-factor spatio-temporal prediction. Specifically, we **first** propose a theoretical solution called the

- J. Ji, Y. Mou, and Z. Wu are with the School of Computer Science and Engineering, Beihang University, Beijing, China.
- J. Wang is with the School of Computer Science and Engineering and School of Economics and Management, Beihang University, Beijing, China.
- C. Long is with the School of Computer Science and Engineering, Nanyang Technological University, Singapore.
- Corresponding author: jywang@buaa.edu.cn

decomposed prediction strategy. Following the divide-and-conquer paradigm, the strategy decomposes the original graph structure that mixes multiple factors into several subgraphs. Then, we can learn relevant ST data on each subgraph separately and integrate them to produce an overall traffic prediction. More importantly, we show that the proposed strategy is theoretically guaranteed to have a smaller prediction error than directly predicting on the original graph. **Next**, we instantiate the strategy as a framework called STGDL, whose key components are automatic graph decomposition and decomposed learning networks. The former component is implemented by matrix masking with two regularization terms preserving the principles of graph completeness and subgraph independence. The latter component is based on forward and backward residual connections and a stack of ST blocks. Each block is responsible for learning ST data on the subgraph relevant to a certain factor. We conduct extensive experiments on four public ST benchmarks including two grid graph-based datasets and two network graph-based datasets. The results show that our STGDL can enhance the performance of a wide range of graph-based ST models by an average of 9.41%. Our contributions are four-fold:

- To our knowledge, this research is pioneering in dealing with the multi-factor issue for ST prediction. In light of this, we introduce a multi-factor ST prediction task and successfully solve it with a theoretically guaranteed portable framework.
- We propose a decomposed prediction strategy to achieve multi-factor ST prediction via graph decomposition in a divide-and-conquer fashion. We prove that the strategy can reduce ST prediction errors.
- We design a portable STGDL framework to instantiate the proposed strategy by automatic graph decomposition and decomposed learning networks. The framework can learn disentangled ST embedding for each latent factor.
- Extensive experiments on four real-world ST datasets exhibit the performance gain achieved by the STGDL plugin on various graph-based ST models. Moreover, a case study confirms that learned patterns can provide interpretability for deep models and their predictions.

The remainder of the paper is organized as follows: Sec. 2 introduces the basic concepts and the problem of multi-factor ST prediction. Sec. 3 proposes a theoretical solution for this problem, while Sec. 4 instantiates it as an ST graph decomposition learning framework. Sec. 5 evaluates the proposed framework using four public datasets with various baselines. The related work and conclusion are presented in Sec. 6 and 7, respectively.

2 PRELIMINARIES

This section gives the basic concepts and introduces the problem definition.

Definition 1 (Spatio-Temporal Graph). A *spatio-temporal (ST) graph* is defined as $\mathcal{G}^{(t)} = (G, \mathbf{X}^{(t)})$. The **graph structure** is represented as $G = (\mathcal{V}, \mathcal{E}, \mathbf{A})$, where \mathcal{V} is a set of nodes with the size of $|\mathcal{V}| = N$, and \mathcal{E} is a set of edges connecting two nodes in \mathcal{V} . $\mathbf{A} \in \mathbb{R}^{N \times N}$ denotes the adjacent matrix of graph G . The **graph signal** $\mathbf{X}^{(t)} \in \mathbb{R}^{N \times F}$ denotes the ST observations defined on G at the t -th time slot, where F is the feature channel.

Problem Statement. Let $\mathcal{G}^{(t-T:t)} = (G, \mathbf{X}^{(t-T:t)})$ be the past ST data with time window T . The key of most ST prediction methods, including ours, is to derive an ST model $f(\cdot)$ to forecast the future evolution of ST data, *i.e.*, $\mathbf{X}^{(t+1)} = f(\mathcal{G}^{(t-T:t)})$. In this work, we reformulate the problem as *multi-factor spatio-temporal prediction*. It aims to learn a multi-factor ST model $f(\cdot) = \{f_k(\cdot)\}_{k=1}^K$, where K is the number of latent factors. Consequently, $\mathbf{X}^{(t+1)}$ is expected to consist of K independent components, *i.e.*, $\mathbf{X}^{(t+1)} = \sum_{k=1}^K \mathbf{X}_k^{(t+1)}$, where $\mathbf{X}_k^{(t+1)} = f_k(\mathcal{G}^{(t-T:t)})$. The k -th component $\mathbf{X}_k^{(t+1)}$ is for characterizing the aspect of $\mathcal{G}^{(t-T:t)}$ that is relevant to the k -th latent factor.

3 DECOMPOSED PREDICTION STRATEGY

In this section, we first provide a theoretical solution for the multi-factor ST prediction problem via a divide-and-conquer paradigm. It is called the decomposed prediction strategy. Then, we prove the effectiveness of the proposed strategy.

3.1 Strategy Framework

ST Data Generation Perspective. From the data generation perspective, the generation process of ST data can be affected by multiple latent factors related to natural phenomena or human socioeconomic activities. Assuming there are K factors, the ST graph data \mathcal{G} can be regarded as a mixture of all $\mathcal{G}_k = (G_k, \mathbf{X}_k), k \in [1, K]$. We use \mathcal{G}_k to denote the ST graph affected by the k -th latent factor. This effect involves two aspects: graph structure G and graph signal \mathbf{X} . Intuitively, we should decouple the graph structures corresponding to different factors, and then model the graph signal under the impact of each factor separately.

Steps of Decomposed Prediction Strategy. Since our decomposed prediction strategy is in the framework of the divide-and-conquer approach, there are three steps in our proposed strategy as in Tab. 1. Details are in the following.

- **Graph decomposition.** The ST graph structure $G = (\mathcal{V}, \mathcal{E}, \mathbf{A})$, containing a mixture of different latent factors, is decomposed into several subgraphs $\{G_k\}_{k=1}^K$. The subgraph $G_k = (\mathcal{V}_k, \mathcal{E}_k, \mathbf{A}_k)$ characterizes the k -th latent factor. There are two constraints in the decomposition process: graph completeness $\bigcup \mathcal{E}_k = \mathcal{E}$, and subgraph independence $\bigcap \mathcal{E}_k = \emptyset$.
- **Decomposed learning.** We learn the relevant ST graph signal data \mathbf{X}_k over G_k separately by a factor-specific ST encoder $f_k(\cdot)$.
- **Prediction integration.** We integrate the partial prediction results corresponding to each latent factor and obtain the overall ST prediction via $\mathbf{X} = \sum_{k=1}^K \mathbf{X}_k$.

Advantage of Decomposed Prediction Strategy. The proposed strategy can reduce the difficulty of the ST prediction problem, and thus produce smaller errors. Specifically, directly modeling the ST data generated by multiple complex factors will result in the stacking of uncertainties from different factors, which reduces the *predictability* of ST data [5], [27], [28]. This will make the ST prediction problem more difficult and thus degrade the model performance. In

TABLE 1
Analogy from the decomposed prediction strategy to divide-and-conquer approach.

Graph decomposition	→	Divide
Decomposed learning	→	Conquer
Prediction integration	→	Combine

contrast, inspired by the divide-and-conquer approach, the decomposed prediction strategy can characterize the impact of each latent factor separately. It makes the partial ST data \mathbf{X}_k over the decomposed k -th subgraph easier to model than the data over the original graph structure, *i.e.*, \mathbf{X} . In this way, we obtain an easier problem, namely *multi-factor ST prediction*. The advantage of the proposed strategy is summarized in the following theorem.

Theorem 1. *Assume the error lower bound of an ST prediction problem is E_o . After introducing the decomposed prediction strategy and transforming the original problem into a multi-factor ST prediction problem, we can have an error lower bound E_d with $E_d < E_o$.*

In Thm. 1, a smaller error lower bound means the difficulty of the corresponding problem is lower, while a low-difficulty problem indicates that it can be solved with smaller errors. The proof of Thm. 1 is provided in the following part.

3.2 Theoretical Analysis

We here prove the advantage of our decomposed prediction strategy given in Thm. 1. As shown in Tab. 1, our strategy includes three steps related to three parts of the divide-and-conquer approach. Therefore, we first transform these three parts into three following lemmas and then prove Thm. 1.

Lemma 1 (Divide). *The graph decomposition step divides the original ST prediction problem into a number of subproblems that are smaller and independent instances of the original problem.*

Lemma 2 (Conquer). *The decomposed learning step conquers the subproblems by solving them separately. The error lower bound of the k -th subproblem is $2e_k\sigma_k^2$. e_k is the lower bound of error rate, and σ_k^2 is the variance of the ST random variable X_k corresponding to the k -th subproblem.*

Lemma 3 (Combine). *The prediction integration step combines the results of the subproblems into the solution for the original problem. The error lower bound of the combined solution is $E_d = \sum_{k=1}^K 2e_k\sigma_k^2$.*

The proof of the three lemmas can be found in Appx. A. Before we delve into the proof of Thm. 1, we have to emphasize that the error rate lower bound of the original ST prediction problem e satisfies

$$\forall k \in [1, K], e_k < e, \quad (1)$$

where e_k is the error rate lower bound of the k -th subproblem, which defines the minimal probability of making incorrect predictions. Eq. (1) is proved in Appx. B by using information entropy and predictability [29], [30]. Next, we give the proof of Thm. 1.

Proof: Assume the error lower bound of the original ST prediction problem P is E_o . From Lemma 2, we know that E_o can be defined as

$$E_o = 2e\sigma^2, \quad \text{s. t.} \quad \sigma^2 = \sum_{k=1}^K \sigma_k^2 \quad (2)$$

where e is the error rate lower bound of directly solving the original ST prediction problem. σ^2 is the variance of the ST random variable X corresponding to the original problem P . The constraint $\sigma^2 = \sum_{k=1}^K \sigma_k^2$ is derived from Lemma 1. Because the original problem is divided into K independent subproblems, the covariance of any two subproblems is zero. This indicates variances of all ST random variables X_k sum up to the variance of X .

Comparing E_d in Lemma 3 and E_o in Eq. (2) with the help of Eq. (1), we have

$$E_d = \sum_{k=1}^K 2e_k\sigma_k^2 < \sum_{k=1}^K 2e\sigma_k^2 = 2e\sigma^2 = E_o. \quad (3)$$

This means that after introducing the decomposed prediction strategy, we can have a smaller error lower bound compared with directly solving the original problem. \square

4 INSTANTIATION FRAMEWORK

Following the principles of the decomposed prediction strategy in Sec. 3, we instantiate a portable Spatio-Temporal Graph Decomposition Learning (STGDL) framework as shown in Fig. 1. In this section, we will elaborate on the STGDL with technical details.

4.1 Overview Framework

Classical data-driven methods model ST data directly based on the original ST graph structure G that is affected by multiple latent factors. Differently, guided by the decomposed prediction strategy, we propose STGDL to model the influence of each factor separately. As illustrated in Fig. 1, our STGDL consists of two main components: *i*) an Automatic Graph Decomposition (AGD) component that corresponds to the first step of the decomposed prediction strategy, and *ii*) a Decomposed Learning Network (DLN) that corresponds to the remaining two steps of the strategy. In AGD, we propose a matrix masking-based automatic method to decompose the original graph into multiple subgraphs. Each subgraph can characterize the graph structure relevant to a certain factor. Details are given in Sec. 4.2.

Over these subgraphs, we design a deep learning model DLN. It stacks several ST blocks by a dual residual mechanism that consists of subtractive and additive residual connections. The former is to disentangle ST data relevant to each ST block, which is relevant to the second step of our strategy. The latter aims to combine partial predictions of every ST block to produce the overall ST prediction. Details of DLN are provided in Sec. 4.3.

In our STGDL, the graph decomposition process is designed to be learnable. Therefore, it can be unified into the same framework with the decomposed learning network. In this way, the whole framework can be easily trained in an end-to-end manner.

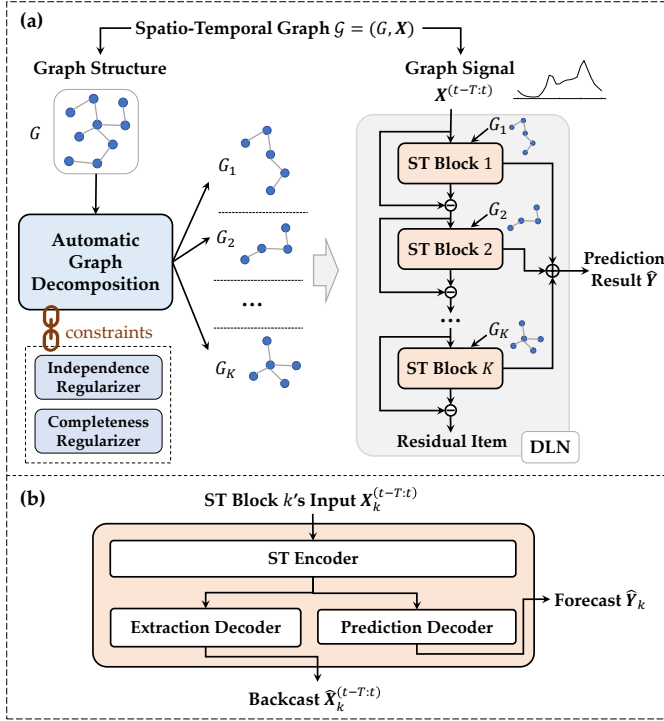


Fig. 1. (a) The architecture of our STGDL framework. The graph structure of the input ST graph is decomposed as several subgraphs via Automatic Graph Decomposition constrained by completeness and independence regularizers. Then, ST graph signals are fed into the Decomposed Learning Network (DLN) for ST prediction corresponding to each subgraph and the overall graph. The residual item of DLN is expected to be zero after subtracting recovered all subgraphs' signals from the input graph signals. (b) An illustration of the ST Block.

4.2 Automatic Graph Decomposition

This part proposes a simple yet efficient graph decomposition scheme. It is implemented by matrix masking and incorporated with two regularization terms preserving the principles of graph completeness and subgraph independence.

4.2.1 Matrix Masking-based Decomposition

Given an original graph structure $G = (\mathcal{V}, \mathcal{E}, \mathbf{A})$ of ST graph data, this module aims to decompose it into a set of subgraphs $\{G_k\}_{k=1}^K$. Specifically, for the k -th subgraph $G_k = (\mathcal{V}_k, \mathcal{E}_k, \mathbf{A}_k)$, we generate the corresponding adjacency matrix \mathbf{A}_k as follows:

$$\tilde{\mathbf{A}}_k = \psi_1(\mathbf{M}_k)\mathbf{A}, \quad (4)$$

where the masking matrix $\mathbf{M}_k \in \mathbb{R}^{N \times N}$ is learnable. The function $\psi_1(\cdot) = (\text{Tanh}(\cdot) + 1)/2$ generate an edge ratio in the range $(0, 1)$. It ensures that the edge weights in $\tilde{\mathbf{A}}_k$ do not exceed that in \mathbf{A} . When \mathbf{A} is a binary adjacency matrix, each item in $\tilde{\mathbf{A}}_k$, i.e., $\tilde{a}_{k,i,j}$, can denote the probability that the relevant edge exists. Compared with heuristic graph decomposition methods [16], [18], [31], [32], our approach is simple, differentiable, and has no restrictions on the type of input graphs.

4.2.2 Regularization Terms

There are two constraints in the graph decomposition step of the decomposed prediction strategy: *i*) the graph

completeness $\cup \mathcal{E}_k = \mathcal{E}$, and *ii*) the subgraph independence $\cap \mathcal{E}_k = \emptyset$. To satisfy both constraints, we introduce two corresponding regularization terms.

Specifically, the *completeness regularizer* \mathcal{L}_c aims to minimize the difference between the original graph and the reconstructed one. It is defined by the graph adjacency matrix as follows:

$$\mathcal{L}_c = \left\| \psi_2(\mathbf{A}) - \psi_2(\hat{\mathbf{A}}) \right\|_1, \quad \text{s.t. } \hat{\mathbf{A}} = \left(\sum_{k=1}^K \mathbf{A}_k \right), \quad (5)$$

where $\|\cdot\|_1$ is the ℓ_1 norm that first flattens the input matrix. $\hat{\mathbf{A}}$ is the reconstructed adjacency matrix of the original graph \mathbf{A} . We use $\psi_2(\cdot)$ to normalize $\hat{\mathbf{A}}$ as a binary matrix. Specifically, we implement it by $\psi_2(x) = (\text{Tanh}(4(x - 0.5)) + 1)/2$.

The *independence regularizer* \mathcal{L}_i aims to maintain the independence between different subgraphs. It is defined as:

$$\mathcal{L}_i = \frac{1}{K(K-1)} \sum_{k=1}^K \sum_{j=1, j \neq k}^K \left\| \mathbf{A}_k^\top \mathbf{A}_j \right\|_1. \quad (6)$$

Minimizing \mathcal{L}_i can steer any pair of adjacency matrices to be orthogonal, thereby making the corresponding subgraphs independent.

4.3 Decomposed Learning Network

The right part of Fig. 1 presents the architecture of the decomposed learning network (DLN). It is comprised of K spatio-temporal blocks and a dual residual mechanism. K is the number of decomposed subgraphs in Sec. 4.2. We briefly overview the framework as follows.

- The *ST block* aims to learn ST data related to the corresponding subgraph. It takes residual historical ST observations of the previous block as input and produces two outputs: predicted ST data and extracted historical ST data. Then, the predicted data of all blocks are integrated for the final forecast, while the extracted historical data are used for backward estimation, *a.k.a.*, backcast.
- The *dual residual mechanism* has two branches: one runs on the backcast of each ST block and the other runs on the overall traffic forecast of all blocks. The former uses subtractive residual connections and the latter is compromised of additive residual connections.

In the following parts, we will illustrate the details of these two components.

4.3.1 Spatio-Temporal Block

As shown in Fig. 1(b), the ST block aims to learn ST data relevant to different subgraphs via backcast and forecast. Formally, the inputs of the k -th ST block are $\mathbf{X}_k^{(t-T:t)} \in \mathbb{R}^{T \times N \times F}$ and the adjacency matrix of k -th subgraph, \mathbf{A}_k . They are mapped by the ST blocks into two outputs:

$$\{\hat{\mathbf{X}}_k, \hat{\mathbf{Y}}_k\} = \text{STB}(\mathbf{X}_k^{(t-T:t)}, \mathbf{A}_k), \quad (7)$$

where $\hat{\mathbf{X}}_k^{(t-T:t)}$ is the estimation of $\mathbf{X}_k^{(t-T:t)}$, and $\hat{\mathbf{Y}}_k \in \mathbb{R}^{N \times 2}$ is the ST data prediction of time step $t+1$, whose ground truth is $\mathbf{X}_k^{(t+1)}$. For the very first ST block in DLN, its respective input $\mathbf{X}_k^{(t-T:t)}$ is the overall model input, i.e., the historical ST data with a lookback window T . For

the rest of the ST blocks, their inputs $\mathbf{X}_k^{(t-T:t)}$ are residual outputs of the previous ST blocks.

Internally, the ST block consists of two parts. The first part is an ST encoder that produces ST embeddings using block inputs. The second part consists of a prediction decoder and an extraction decoder. It uses the ST embeddings to produce the forecast output $\hat{\mathbf{Y}}_k$ and the backcast output $\hat{\mathbf{X}}_k^{(t-T:t)}$. Many deep ST models were proposed to encode ST data as ST embeddings and then make predictions using the embeddings [15], [20], [21]. Therefore, we can directly adopt the encoding subnetworks of these models as our ST encoder, and adopt their forecasting subnetworks as our prediction decoder. As for the extraction decoder, since the main difference between the prediction decoder and the extraction decoder is the output length, we can get the extraction decoder by simply modifying the output length of the prediction decoder.

4.3.2 Dual Residual Mechanism

We introduce a dual residual mechanism to disentangle the partial ST data affected by different latent factors. It consists of two types of residual connections: subtractive and additive residual connections.

The subtractive residual connection removes components of ST block input that are not helpful for ST prediction of the downstream blocks. For the k -th ST block, the subtractive residual connection is defined by

$$\mathbf{X}_k^{(t-T:t)} = \mathbf{X}_{k-1}^{(t-T:t)} - \hat{\mathbf{X}}_{k-1}^{(t-T:t)}, \quad (8)$$

where $\hat{\mathbf{X}}_{k-1}^{(t-T:t)}$ is the backcast of the input of $(k-1)$ -th ST block, *i.e.*, $\mathbf{X}_{k-1}^{(t-T:t)}$. The backcast residual branch $\mathbf{X}_k^{(t-T:t)}$ can be considered as running a disentanglement process of the input ST data. The previous block removes the portion of ST data $\hat{\mathbf{X}}_{k-1}^{(t-T:t)}$ defined on $(k-1)$ -th subgraph, making the prediction task of the downstream blocks irrelevant to $(k-1)$ -th latent factor. In this way, we encourage the ST block to disentangle ST data affected by different factors. To ensure that no additional ST data is left behind, we design a residual loss for the last residual item to be close to zero. It is defined as

$$\mathcal{L}_r = \left\| \mathbf{X}_K^{(t-T:t)} \right\|_1, \quad (9)$$

where $\|\cdot\|_1$ is the ℓ_1 norm that first flattens the input data.

On the other hand, the additive residual connection aggregates the partial ST predictions of every ST block to produce the overall ST prediction. It can be described by

$$\hat{\mathbf{Y}} = \sum_{k=1}^K \hat{\mathbf{Y}}_k. \quad (10)$$

Since this allows for the k -th ST block to focus on the partial ST data affected by the k -th latent factors, we expect accurate predictions of ST data that mix impacts of several latent factors. Eq. (10) also provides a disentanglement of future ST data because all partial predictions can be treated as the decomposition of $\hat{\mathbf{Y}}$. We finally optimize the multi-factor ST prediction task by minimizing the loss function:

$$\mathcal{L}_p = \left\| \hat{\mathbf{Y}} - \mathbf{X}^{(t+1)} \right\|_1. \quad (11)$$

Algorithm 1 Training Algorithm of STGDL

Input: Traffic flow graph data $\{\mathcal{G}^{(1)}, \dots, \mathcal{G}^{(\tau)}\}$.

Output: The learned STGDL model.

```

1: for available  $t \in \{1, \dots, \tau\}$  do
2:    $\mathbf{X} \leftarrow \{\mathbf{X}^{(t-T:t)}, \mathbf{A}\}$ . ▷ Input data
3:    $\mathbf{Y} \leftarrow \mathbf{X}^{t+1}$ . ▷ Label
4:   Put  $\{\mathbf{X}, \mathbf{Y}\}$  into  $\mathcal{D}_{train}$ .
5: Initialize all trainable parameters.
6: while stopping criterion is not met do
7:   Randomly select a batch  $\mathcal{D}_{batch}$  from  $\mathcal{D}_{train}$ .
8:   Forward-backward on  $\mathcal{L}_{joint}$  by  $\mathcal{D}_{batch}$ .
9:   for parameter  $\theta$  in AGD do ▷ AGD is in Sec. 4.2
10:     $\theta = \theta - \alpha \cdot \nabla_{\theta} \mathcal{L}_{joint}$  ▷  $\alpha$  is learning rate
11:   for parameter  $\theta$  in DLN do ▷ DLN is in Sec. 4.3
12:     $\theta = \theta - \alpha \cdot \nabla_{\theta} \mathcal{L}_{joint}$ 
13: return Learned STGDL model.
```

More importantly, with the guidance of expert knowledge, the prediction of each ST block can have its own physical meaning in reality. This can enhance the interpretability of our model's outputs. For example, in ST traffic prediction, the first ST block could be responsible for commuting flow, the second for entertaining flow, and so on.

4.4 Model Training

In the learning process of our STGDL, we calculate the overall loss by incorporating the graph decomposition losses in Eq. (5) and Eq. (6) and the decomposed learning loss in Eq. (11) into the joint learning objection:

$$\mathcal{L}_{joint} = \mathcal{L}_c + \mathcal{L}_i + \mathcal{L}_r + \mathcal{L}_p. \quad (12)$$

Our model can be trained end-to-end via the back-propagation algorithm. The entire training procedure can be summarized into Algo. 1. In lines 1-4, we construct training data. In lines 6-12, we iteratively optimize STGDL by gradient descent until the stopping criterion is met. Specifically, in lines 7-8, we first select a random batch of data and then apply the forward-backward operation on the whole model to get gradients of all parameters. At last, in lines 9-12, we update the parameters within AGD and DLN components by gradient descent respectively.

5 EXPERIMENTS

In this section, we evaluate the effectiveness of STGDL on a series of experiments over four real-world benchmark datasets, which are summarized to answer the following research questions:

- **RQ1:** How is the overall traffic prediction performance of STGDL as compared to various baselines?
- **RQ2:** How effective is the decomposition strategy when ported to various baseline methods?
- **RQ3:** How do the designed different submodules contribute to the model performance?
- **RQ4:** What is the impact of hyper-parameters in STGDL?
- **RQ5:** How do the learned representations of decomposed graphs contribute to model interpretability?

5.1 Experimental Settings

Since urban traffic data is the most typical kind of spatio-temporal data, we test our model mainly based on traffic data and the ST traffic prediction task.

5.1.1 Data Description

We evaluate our model on two types of graph-based public real-world traffic datasets, including grid graph-based datasets and network graph-based datasets. The grid graph-based datasets include a bike dataset and a taxi dataset. Bike data contains bike rental records. Taxi data record the number of taxis coming to and departing from a region given a specific time interval. The network graph-based datasets include two sensor datasets. They are mainly generated by highway sensors that measure the flow volume or the vehicle speed of given roads. These datasets are generated by millions of taxis, bikes, or highway vehicles on average and contain thousands of time steps and hundreds of regions or roads. The statistical information is summarized in Table 2. More details are in the following:

- **NYCBike** is a public traffic flow dataset collected from New York City. Specifically, NYCBike contains bike rental data over a period of six months from 04/01/2014 to 09/30/2014 [11]. We divide New York City into a raster with 16×8 grid zones and map bike records as traffic flow among zones. Traffic flows in NYCBike are measured on an hourly basis, and the total sequence length is 4,392.
- **NYCTaxi** is also a public dataset collected from New York City. Specifically, NYCTaxi contains taxi GPS ranging from 01/01/2015 to 03/01/2015. The city is divided into a grid of 20×10 to map taxi trajectories as traffic flow among zones [17]. It is measured every 30 minutes, and the total sequence length is 2,880.
- **PEMSD7(M)** is a public traffic dataset collected from California Performance of Transportation (PeMS) [33]. Specifically, it contains data from 228 sensors in District 07 over a period of 2 months from 05/01/2012 to 06/30/2012 [20]. The traffic information is recorded every 5 minutes. We aggregate them on a 30-minute basis and obtain 2,112 sequences.
- **PEMSD8** is a public traffic dataset collected from PeMS. Specifically, it contains data from 170 sensors in District 08 over a period of 2 months from 07/01/2018 to 08/31/2018 [12]. The traffic information is originally recorded every 5 minutes. We aggregate them in 30 minutes and obtain 2,976 sequences.

For all datasets, previous 2-hour flows and previous 3-day flows around the predicted time are used to predict the flows for the next time step. This can facilitate the modeling of shifted temporal correlations [17]. A sliding window strategy is utilized to generate samples. Then, we split each dataset into the training, validation, and test sets with a ratio of 7:1:2.

Construction of ST Graph Structure. For grid graph-based datasets (*i.e.*, NYCBike and NYCTaxi), to distinguish the weights of edges between different nodes, we compute the dynamic time warping (DTW) distance of traffic series between nodes as the adjacency matrix. Specifically, the element a_{ij} of the adjacency matrix \mathbf{A} is computed by $a_{ij} = \text{DTW}(\mathbf{x}_i, \mathbf{x}_j)$, where \mathbf{x}_i denotes the time series for node i , and r is a pre-defined threshold that determines the sparsity of the resulting adjacency matrix. For network graph-based datasets (*i.e.*, PEMS7(M) and PEMS8), we compute the pairwise road network distances between

TABLE 2
Statistics of all four datasets.

Data type	Grid graph		Network graph	
Dataset	NYCBike	NYCTaxi	PeMSD7(M)	PeMSD8
Time interval	1 hour	30 min	30min	30min
# graph nodes	128	200	228	170
seq. length	4,392	2,880	2,112	2,976

sensors and build the adjacency matrix using thresholded Gaussian kernel [14].

5.1.2 Evaluation Metrics & Baselines

We adopt three commonly used metrics to measure the accuracy of the prediction results, including Mean Average Error (MAE), Mean Absolute Percentage Error (MAPE), and Rooted Mean Square Error (RMSE). As for the baselines, we first compare our STGDL with two classic non-deep models, including:

- **HA**: Historical Average models ST data as a seasonal process and calculates the average of data as prediction results.
- **SVR**: Support Vector Regression is a regression model using a linear support machine. It is a traditional machine learning method.

Secondly, we implement five deep learning models proposed in recent years to compare with our STGDL.

- **STGCN** [20]: Spatio-Temporal Graph Convolution Network is a graph convolution-based model that uses 1D convolution to capture spatial dependencies and temporal correlations.
- **GWNet** [15]: GWNet is short for graph-wavenet that combines diffusion graph convolution with dilated causal convolution to capture spatial-temporal dependencies.
- **MTGNN** [34]: Multivariate Time series forecasting with Graph Neural Networks employs adaptive graphs and integrates GRU with graph convolutions.
- **MSDR** [35] Multi-step Dependency Relation Networks is an RNN-based model that explicitly takes hidden states of multiple historical steps as the input of each time unit.
- **STSSL** [21]: Spatio-Temporal Self-Supervised Learning is a self-supervised model that designs two auxiliary tasks to learn effective region embeddings for traffic prediction.

For the deep learning baselines, we implement them based on the released codes of the LibCity [36] benchmark¹, which integrates a great number of ST forecasting models according to their original paper. Note that all these deep models can be considered as combinations of ST encoders and ST decoders. They can be used as backbone models and integrated with our STGDL framework. Next, we give the settings of STGDL in detail.

5.1.3 Parameter Settings

The STGDL is implemented with Python 3.9 and PyTorch 1.12.0. The number of subgraphs is searched from the range of $\{4, 5, 6, 7, 8, 9, 10\}$ for all datasets. We found the optimal settings are 6, 6, 6, 8 for NYCBike, NYCTaxi,

1. <https://github.com/LibCity/Bigscity-LibCity>

TABLE 3

ST prediction on two grid graph-based traffic datasets, *i.e.*, NYCBike and NYCTaxi, in terms of MAE, MAPE (%), and RMSE. In and Out represents the inflow and outflow. “Improv.” measures the improvement of STGDL over the counterpart baseline with respect to each task and each metric.

Dataset	NYCBike						NYCTaxi					
	MAE		MAPE		RMSE		MAE		MAPE		RMSE	
Type	In	Out	In	Out	In	Out	In	Out	In	Out	In	Out
HA	10.85	11.09	45.68	46.98	16.91	17.50	36.76	28.51	46.72	44.02	66.87	56.68
SVR	8.48	8.59	34.63	34.63	13.67	14.31	35.81	28.65	45.62	43.47	68.91	58.05
STGCN	5.26±0.02	5.53±0.04	22.58±0.29	23.13±0.38	7.65±0.05	8.23±0.11	12.87±0.21	10.93±0.13	17.13±0.16	17.23±0.2	23.09±0.5	23.62±0.47
STGCN+	5.07±0.05	5.36±0.02	21.77±0.08	22.55±0.05	7.36±0.11	7.95±0.07	11.84±0.12	9.68±0.15	17.14±0.84	16.80±0.01	21.17±0.26	17.61±0.79
Improv.	+3.61%	+3.07%	+3.59%	+2.51%	+3.79%	+3.40%	+8.00%	+11.44%	-0.06%	+2.50%	+8.32%	+25.45%
GWNet	5.15±0.02	5.43±0.02	22.67±0.21	23.24±0.20	7.38±0.03	8.01±0.04	12.7±0.02	10.39±0.08	17.45±1.12	17.79±0.48	22.48±0.06	18.29±0.12
GWNet+	4.97±0.02	5.25±0.01	21.61±0.21	22.28±0.02	7.12±0.04	7.75±0.05	11.53±0.08	9.32±0.04	15.78±0.21	16.28±0.32	20.57±0.21	16.15±0.07
Improv.	+3.50%	+3.31%	+4.68%	+4.13%	+3.52%	+3.25%	+9.21%	+10.30%	+9.57%	+8.49%	+8.50%	+11.70%
MTGNN	5.26±0.03	5.57±0.03	22.77±0.10	23.83±0.61	7.68±0.06	8.31±0.03	12.71±0.03	10.19±0.03	17.03±0.06	17.71±0.25	22.37±0.05	18.0±0.12
MTGNN+	5.12±0.01	5.42±0.01	22.28±0.13	23.18±0.03	7.46±0.04	8.12±0.02	11.94±0.15	9.71±0.09	16.38±0.36	16.98±0.47	21.07±0.26	16.9±0.19
Improv.	+2.66%	+2.69%	+2.15%	+2.73%	+2.86%	+2.29%	+6.06%	+4.71%	+3.82%	+4.12%	+5.81%	+6.11%
MSDR	5.65±0.10	6.00±0.14	24.54±0.59	25.89±0.10	8.26±0.15	8.99±0.23	18.49±1.20	15.89±1.02	25.27±1.73	25.78±1.93	33.7±2.09	33.17±1.67
MSDR+	5.25±0.05	5.55±0.07	23.22±0.24	23.86±0.30	7.68±0.11	8.31±0.10	14.72±0.10	11.53±0.28	20.61±1.00	20.37±0.64	26.31±0.34	21.44±0.63
Improv.	+7.08%	+7.50%	+5.38%	+7.84%	+7.02%	+7.56%	+20.39%	+27.44%	+18.44%	+20.99%	+21.93%	+35.36%
STSSL	5.18±0.03	5.44±0.02	22.37±0.17	23.00±0.21	7.56±0.06	8.15±0.03	12.19±0.14	10.0±0.09	16.43±0.04	17.06±0.17	21.7±0.28	19.05±0.37
STSSL+	5.10±0.04	5.37±0.04	22.36±0.10	22.99±0.26	7.45±0.14	8.03±0.16	11.83±0.10	9.74±0.14	16.36±0.01	17.11±0.30	20.86±0.22	17.06±0.43
Improv.	+1.54%	+1.29%	+0.04%	+0.04%	+1.46%	+1.47%	+2.95%	+2.60%	+0.43%	-0.29%	+3.87%	+10.45%

PEMSD7(M), and PEMS8. The batch size is set to 32. The model training phase is performed using the Adam optimizer with the learning rate set as 0.001. The hidden dimension is determined by the different backbone models. For any more details, readers could refer to our public code repository ².

5.2 Performance Comparison (RQ1 & RQ2)

In this part, we report and analyze the traffic forecasting performance of non-deep models, base deep models, and enhanced deep models over grid graph-based datasets (Tab. 3) and network graph-based datasets (Tab. 4). For simplicity, we name the deep models enhanced by our STGDL as “base model+”. We ran all deep models and their enhanced versions with five different random seeds, and then reported the average performance and its standard deviation, shown as “mean±standard deviation”.

5.2.1 Results on Grid Graph-Based Datasets

Tab. 3 shows the comparison results on grid graph-based datasets, including NYCBike and NYCTaxi.

Performance Superiority of STGDL. We first compare the enhanced deep models by our STGDL with their basic version. On average, the enhanced models have 3.63% MAE improvement, 3.31% MAPE improvement, and 3.66% RMSE improvement in NYCBike, as well as 10.31% MAE improvement, 6.80% MAPE improvement, and 13.75% RMSE improvement in NYCTaxi. The enhanced model GWNet+ performs the best among all methods. It is worth noting that the overall improvement in the NYCTaxi dataset is about twice that of the NYCBike dataset. The reason for

this phenomenon is that there are more traffic participants in NYCTaxi (22m+) compared to NYCBike (6.8k+). This produces traffic patterns affected by more complex factors in NYCTaxi, compared with NYCBike. In this case, STGDL learns the factor-specific patterns by a decomposed prediction strategy, enabling higher performance gains. In the case of NYCBike, where traffic patterns are simple, the original model can achieve good performance using powerful deep learning techniques, so the performance improvement of STGDL is insignificant. As a result, our STGDL provides a greater performance boost to deep models on NYCTaxi compared to NYCBike.

Performance Comparison between Baselines. We can observe that *i)* Conventional non-deep models, including ARIMA and SVR, are not good enough to predict traffic flows, because of the limitation of the model expressiveness that is unable to capture complex and dynamic ST correlations. *ii)* Compared with non-deep models, deep models deliver better forecasting performance, because they exploit a wide variety of deep learning techniques to target the learning of high-quality ST representations.

5.2.2 Results on Network Graph-Based Datasets

Tab. 3 shows the comparison results on network graph-based datasets, including PEMS7(M) and PEMS8.

Performance Superiority of STGDL. We first compare the enhanced deep models by our STGDL with their basic version. On average, the enhanced models have 7.56% MAE improvement, 7.80% MAPE improvement, and 4.46% RMSE improvement in the PEMS7(M) dataset, as well as 17.96% MAE improvement, 18.33% MAPE improvement, and 15.31% RMSE improvement in the PEMS8 dataset. Compared to grid graph-based datasets, the results on net-

2. <https://github.com/bigcity/STGDL>

TABLE 4
Traffic forecasting on two network graph-based datasets, *i.e.*, PEMS7(M) and PEMS8, in terms of MAE, MAPE (%), and RMSE.

Dataset	PEMS7(M)			PEMS8		
	MAE	MAPE	RMSE	MAE	MAPE	RMSE
HA	4.62	11.77	7.50	36.89	24.66	53.99
SVR	3.23	8.72	6.14	30.90	18.39	47.10
STGCN	2.15±0.01	5.14±0.07	4.25±0.03	11.56±0.25	8.25±0.13	19.55±0.60
STGCN+	2.04±0.01(+5.12%) ¹	4.88±0.01(+5.06%)	4.16±0.01(+2.12%)	8.70±0.03(+24.74%)	6.72±0.05(+18.55%)	14.67±0.07(+24.96%)
GWNet	2.13±0.01	5.01±0.02	4.22±0.02	9.63±0.06	7.31±0.12	15.97±0.11
GWNet+	2.04±0.01(+4.23%)	4.82±0.04(+3.79%)	4.17±0.01(+1.18%)	8.34±0.06(+13.4%)	6.24±0.27(+14.64%)	14.38±0.07(+9.96%)
MTGNN	2.06±0.01	4.82±0.01	4.15±0.02	8.93±0.07	7.54±0.50	15.17±0.06
MTGNN+	2.04±0.02(+0.97%)	4.78±0.05(+0.83%)	4.15±0.01(+0.00%)	8.27±0.03(+7.39%)	6.46±0.13(+14.32%)	14.54±0.07(+4.15%)
MSDR	3.40±0.07	8.49±0.29	6.19±0.22	17.78±1.10	15.38±1.78	28.03±1.64
MSDR+	2.53±0.19(+25.59%)	6.19±0.57(+27.09%)	5.00±0.40(+19.22%)	14.45±0.66(+18.73%)	12.20±0.98(+20.68%)	23.43±1.45(+16.41%)
STSSL	2.09±0.02	4.98±0.03	4.19±0.02	10.77±0.02	7.97±0.20	18.01±0.08
STSSL+	2.05±0.01(+1.91%)	4.87±0.03(+2.21%)	4.20±0.01(-0.24%)	8.02±0.05(+25.53%)	6.10±0.18(+23.46%)	14.22±0.04(+21.04%)

¹ The percentage measures the improvement of STGDL over the counterpart baseline with respect to one metric, *e.g.*, MAE.

work graph-based datasets are more promising. Notably, when applying our STGDL on MTGNN, the best base model, it can still significantly improve the MAE (7.39%), MAPE (14.32%), and RMSE (4.15%) in the PEMS8 dataset. The reason behind this is that PEMS8 has 170 sensors corresponding to many highway roads, and they may be responsible for different functions. Therefore, a model collectively learning mixed data evolution patterns cannot effectively capture such diverse ST traffic trends. Instead, our STGDL employs a decomposed learning network to learn different evolution trends individually, enabling the model to better capture the mixed ST patterns. As a result, the deep models enhanced by STGDL can have much better performance than the basic versions.

Performance Comparison between Baselines. First, non-deep models still produce unsatisfactory ST traffic prediction performance on network graph-based datasets, showing their limitations for modeling complex real-world ST data. Second, with the boost of advanced deep learning techniques, deep models generate better results compared to non-deep ones. Interestingly, for the base version, the performance ranking of the best three models is MTGNN > GWNet > STSSL, but the ranking shows as STSSL+ > GWNet+ > MTGNN+ when enhanced by STGDL. This suggests that STGDL has different enhancement effects for different types of deep models.

5.3 Ablation Study (RQ3)

To verify the effectiveness of submodules in STGDL, we conduct ablation studies on all four datasets regarding three important submodules. They include automatic graph decomposition, regularization terms for decomposition, and the decomposed learning network. There are five models enhanced by our STGDL, we only report the results of STGCN in this part because other models exhibit a similar phenomenon. For clarity, we use STGDL to denote the enhanced deep models.



Fig. 2. Effectiveness of the automatic graph decomposition *w.r.t.* MAE.

5.3.1 Effectiveness of Automatic Graph Decomposition

Before we delve into the ablation study on automatic graph decomposition, we first introduce some background of graph decomposition. Graph decomposition method, *a.k.a.*, graph partitioning, can be categorized into node decomposition method and edge decomposition method according to the way of splitting the input graph data [37], [38]. The node decomposition method aims to assign the graph nodes to each subgraph and maintain edges between nodes of the same subgraph [32]. This may cause edges between different subgraphs to be cut off, thereby destroying the original graph structure. Differently, the edge decomposition method assigns the edges of the input graph to each subgraph, and each group of assigned edges constitutes a subgraph [31], which may lead to the redundancy of boundary nodes but maintain the original graph structure.

In Sec. 4.2, we introduced an Automatic Graph Decomposition (AGD) method, which belongs to the category of edge decomposition. In order to verify its effectiveness, we designed three variants using traditional decomposition methods or even removing the decomposition module. We describe their details in the following.

- **TED:** A Traditional Edge Decomposition (TED) algorithm is employed to generate the subgraphs for each ST block. Here we choose a classic method called degree-based hashing [31] which assigns each edge by hashing the identification of its end-vertex with a lower degree.
- **TND:** A Traditional Node Decomposition (TND) algo-

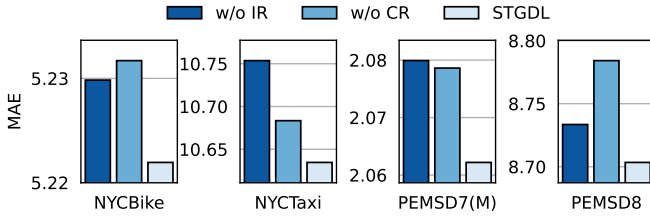


Fig. 3. Effectiveness of regularization terms *w.r.t.* MAE.

rithm is used for subgraph generation for each ST block. We choose spectral clustering [32] which groups graph nodes using eigendecomposition of the Laplacian matrix of the input graph.

- **w/o AGD:** We remove the AGD submodule, and we use the original graph as the input graph for each ST block.

The results are presented in Fig. 2. Primarily, we can observe that the performance ranking is $TND < TED < STGDL$ in most cases, which shows the superiority of the automatic method. Because the ST data vary with time, the static decomposition approach cannot effectively capture the dynamic correlation between different graph nodes, thereby delivering unsatisfactory results. In contrast, our STGDL can capture such dynamics via the data-driven automatic decomposition method and produces good performance. On the other hand, TND is beaten by TED in most cases. This illustrates the importance of maintaining a complete graph structure in ST prediction, hence we chose the edge decomposition paradigm over the node decomposition paradigm. Moreover, w/o AGD always performs worse than STGDL. This indicates the necessity of decomposition, without which a model is unable to decompose the ST traffic data relevant to multiple latent factors. Instead, it directly performs mixed-factor ST prediction that is complicated, leading to worse performance compared with STGDL. By combining the automatic fashion and edge decomposition method, our STGDL produces the best performance.

5.3.2 Effectiveness of Regularization Terms

There are two constraints within the decomposed prediction strategy, including graph completeness and subgraph independence. To this end, we design two regularization terms for automatic graph decomposition, *i.e.*, completeness regularizer \mathcal{L}_c in Eq. (5) and independence regularizer \mathcal{L}_i in Eq. (6), to satisfy these constraints. To examine their effectiveness, we prepared two variants as follows.

- **w/o IR:** The independence regularizer \mathcal{L}_i is removed.
- **w/o CR:** The completeness regularizer \mathcal{L}_c is removed.

The results are shown in Fig. 3. It can be observed that across all four datasets, the predictive accuracy of the two variants without regularization terms is inferior to that of the original model. This verifies the significant role of both regularization terms. Specifically, the objective of \mathcal{L}_i is maximizing the sum of dot products between adjacency matrices of different subgraphs. This ensures the distinctiveness between subgraphs and orthogonality among the subproblems relevant to each subgraph, thereby enforcing different ST blocks to focus on different data evolution patterns. Removing \mathcal{L}_i would result in the non-orthogonality

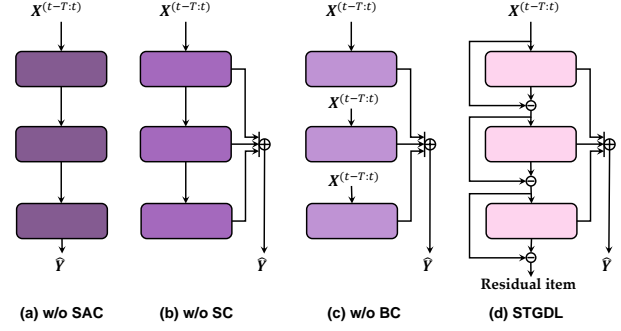


Fig. 4. Illustration of variants about the dual residual mechanism. Without loss of generality, we take three ST blocks as an example. There can be more blocks in practice.

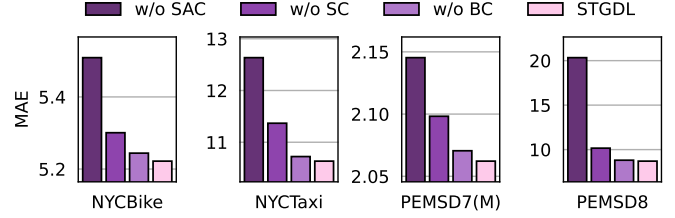


Fig. 5. Effectiveness of the decomposed learning network *w.r.t.* MAE.

of the subproblems, violating the orthogonality constraint and leading to performance degradation. On the other hand, the completeness regularizer \mathcal{L}_c aims to ensure that every edge in the original graph is present in some decomposed subgraph. Eliminating \mathcal{L}_c would cause certain edges from the original graph to be absent in any subgraphs, resulting in information loss and, consequently, a decline in ST prediction performance.

5.3.3 Effectiveness of Decomposed Learning Network

In the decomposed learning network (Sec. 4.3), we design a dual residual mechanism to disentangle ST data. The mechanism includes additive and subtractive residual connections among ST blocks. The additive ones are designed for integrating partial ST predictions of each block for the overall result. The subtractive ones are designed for removing data patterns that have been learned by the backcast process of the previous ST block. These patterns do not contribute to the ST prediction of downstream blocks. To verify the effectiveness of this mechanism, we designed three variants to compare with our STGDL in the following.

- **w/o BC:** The backcast part in the ST block is removed, and we use the original input data as the input for each ST block.
- **w/o SC:** The subtractive connections are removed. We feed the output of the previous ST block as the input of the current ST block.
- **w/o SAC:** The subtractive and additive connections are both removed, which means the dual residual mechanism is dropped. This variant simply stacks several ST blocks.

To facilitate understanding, we illustrate all three variants and STGDL in Fig. 4. The comparison results are depicted in Fig. 5. First, STGDL consistently outperforms w/o SAC with a large margin, indicating the effectiveness

of our dual residual mechanism. Since ST data are usually affected by different latent factors, without this mechanism, w/o SAC struggles to make accurate predictions for traffic ST data that mix the impact of several factors. It is worth noting that the dual residual mechanism not only solves the problem of multi-factor ST data modeling, but also brings *better model scalability*. This allows ordinary ST models to go deeper, thus preparing for large ST models.

Second, the performance of other variants, *i.e.*, w/o BC and w/o SC that have modified the data propagation process, is lower than that of the original model. This verifies the importance of designing a proper data flow in model architecture. Recall the subtractive connections are responsible for eliminating data components affected by the current block-specific factor. Since this portion of data is irrelevant for downstream blocks, subtractive connections can facilitate downstream ST prediction. However, w/o BC feeds all ST blocks with the original input data, forcing each ST block to extract relevant data components from the complex and mixed original data distribution. In contrast, only the first ST block needs to do that in our STGDL, and the extraction complexity of the remaining ST blocks is linearly decreasing. This facilitates the learning efficiency. As for the variant w/o SC, it replaces the subtractive connections with the regular connections, so the model must learn both the extraction operation and the subtraction operation simultaneously. The results in Fig. 5 show that this severely burdens the model learning and makes the prediction accuracy drop significantly.

5.4 Parameter Sensitivity (RQ4)

In this part, we conduct experiments to analyze the impact of the only hyper-parameter in STGDL, *i.e.*, subgraph number K . We vary K in the range of $\{4, 5, 6, 7, 8, 9, 10\}$ for all four datasets. We use MAE as the default metric and STGCN as the default base model. The results are shown in Fig. 6. The optimal choice of K is 6, 6, 6, and 8 for NYCBike, NYCTaxi, PEMS7(M), and PEMS8 respectively. As we can see from the results, having too few subgraphs can seriously affect the performance because it fails to capture the effects of multiple factors. Too many subgraphs may lead to overfitting, which reduces the prediction accuracy. When applying $K = 9, 10$ for the first three datasets, the performance drops significantly so we omit them in Fig. 6.

5.5 Case Study (RQ5)

Next, we visualize the learned ST embeddings and predicted ST data evolution as case studies. The showcases highlight two advantages of our proposed STGDL framework: *i)* it can decompose the embedding space for latent factors that have an impact on ST data, and *ii)* the predicted partial results corresponding to each factor can well explain the final overall predictions. Note that we use STGCN as the default base model in our case study for the balance of performance and efficiency.

5.5.1 Decomposed Embedding Space for Latent Factors

In the decomposed learning network (Sec. 4.3), there are several ST blocks that aim to learn partial ST data relevant to different latent factors. Each ST block first generates ST

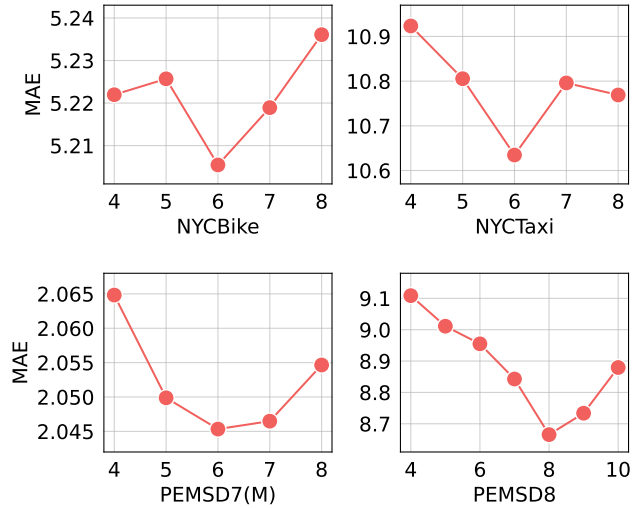


Fig. 6. Evaluation on the number of subgraphs K w.r.t. MAE. The optimal choice of K for NYCBike, NYCTaxi, PEMS7(M), and PEMS8 is 6, 6, 6, and 8, respectively.

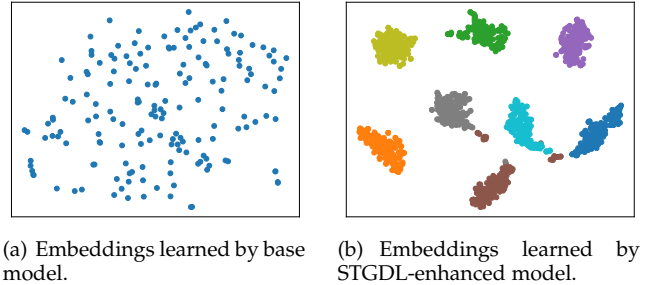
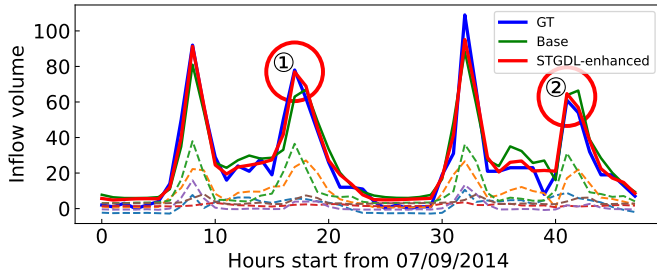


Fig. 7. Visualization of the learned ST embeddings.

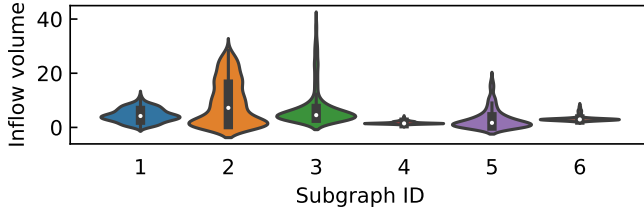
embeddings of the input data by an ST encoder, and then the embeddings are used for backcast and forecast. Only if the ST embeddings capture meaningful features for each latent factor, we can make accurate ST prediction. To explore whether our STGDL could learn quality embeddings, we visualize the learned embeddings of PEMS8 by t-SNE. We randomly select a traffic ST data sample for visualization. The learned embeddings of the base model and the STGDL-enhanced version are shown in Fig. 7(a) and (b), respectively. In these figures, each scatter denotes a node embedding of the traffic ST graph.

We can observe that the ST embeddings generated by the base model are relatively dispersed in the feature space, with no obvious patterns found. In contrast, the ST embeddings learned by our STGDL-enhanced model are significantly better categorized into 8 clusters. For better understanding, we use different colors to indicate the embedding of different decomposed subgraphs. We can find that each cluster corresponds to a subgraph that represents a certain latent factor. This is because the STGDL is designed for modeling the multi-factor ST prediction task. That is, each set of embeddings serves a downstream task that corresponds to a specific factor and therefore exhibits a degree of intrinsic similarity.

Furthermore, we delve into the embeddings of each cluster. These enhanced embeddings, in contrast to those generated by the base model, tend to exhibit a stronger alignment along a *one-dimensional axis* in a small area of the feature space (taking the orange cluster as an example). This



(a) Prediction visualization. The solid blue line represents the ground truth (GT). The solid green line and solid red line represent the predictions of the base model and the STGDL-enhanced model, respectively. The dashed lines represent the predictions on 6 subgraphs within the enhanced model.



(b) Data distribution of predictions on 6 subgraphs.

Fig. 8. Interpretability analysis of the prediction results.

alignment indicates a greater focus on modeling a singular factor within the input ST data, thereby demonstrating the necessity of our framework in decoupling the original ST prediction problem into multiple problems relevant to different latent factors.

5.5.2 Interpretation for Traffic Prediction Results

Here, we show the interpretability potential of our STGDL's predictions and its internal mechanism by visualizing the prediction results.

From the model aspects, Fig. 8(a) illustrates a typical case on the NYCBike dataset, focusing on node 80, during a 48-hour period starting from 00:00 on 07/09/2014. We visualize the prediction results of STGDL-enhanced model and the base model. It can be observed that the enhanced model produces more accurate predictions, especially in peak hours, compared to the base model. To explain this, we plot the predicted data evolution on 6 subgraphs. It is these partial data components that contribute to the final ST prediction of the STGDL-enhanced model, so they can be used as an interpretation for model predictions. Specifically, at point ①, the prediction of the base model and that of the subgraph (dashed orange line) exhibit similar *bimodal* trends. However, due to the influence of other factors (such as factors corresponding to the dashed light green line), the actual data distribution should be *unimodal*. Consequently, the predictions of the STGDL-enhanced model are more accurate than the basic counterpart. A similar interpretation example can also be found at point ②.

As for the internal mechanism, our STGDL aims to make multi-factor ST prediction by forecasting partial ST data under different factors separately. This means that the prediction results of different ST blocks are supposed to be distinct. As shown in Fig. 8(b), the data distributions of ST predictions under different factors vary greatly. This

indicates that our STGDL successfully captures the patterns of different latent factors. We believe that guided by some expert knowledge or data, our STGDL can learn ST patterns that have real-world physical meaning.

6 RELATED WORK

Spatio-Temporal Prediction has drawn great attention in recent years due to its integral role in intelligent decision-making, scheduling, and management in smart cities [39], [40], [41]. To simultaneously model the temporal and spatial dependencies, most studies adopt deep learning techniques. For temporal dependency modeling, they employ the recurrent neural networks [14], [19], [35], temporal convolutional networks [15], [16], [18], or attention mechanism [17]. For spatial dependency modeling, they utilize graph neural networks [4], [20], [21], [34] or attention mechanism over graphs [3], [16], [42], [43]. These models focus on designing a holistic model to capture all spatio-temporal patterns affected by multiple latent factors, making it challenging to accurately predict the evolution of spatio-temporal data. To overcome this limitation, we re-formulate the learning task as a multi-factor spatio-temporal prediction problem. We then incorporate graph decomposition to model multiple subgraphs relevant to different latent factors, effectively capturing the influence of multiple latent factors.

Graph Decomposition, or graph partitioning, is a pivotal task in graph theory that involves decomposing complex input graphs into simpler subgraphs [37]. The primary goal is to delve into the graph's organization and features more effectively, and the optimization objective is to divide the graph into balanced partitions while minimizing the cut across the partitions [38]. Due to its combinatorial nature, many approximate algorithms have been developed, including multilevel partitioning [44], spectral clustering [32], pagerank-based local partitioning [45], simulated annealing [46] and more. Recent advances in graph decomposition have seen the integration of deep learning techniques, including GAP [47] which learns node embeddings and designs specific loss functions for the optimizing objective. Graph partitioning is primarily applied in high-performance parallel computing. In the domain of spatio-temporal traffic forecasting, Ref. [48] partitions the graph into multiple parts to process DCRNN [14] on a large graph. However, in the aspect of decoupling spatio-temporal data, there is currently a lack of research and application of graph decomposition. To leverage the advantage of graph decomposition, we attempt to apply it to traffic prediction for modeling the impact of multiple factors. Unlike classical methods, the graph decomposition strategy we employ is not aimed solely at minimizing the cuts between subgraphs. Instead, it is integrated as a learnable module within our STGDL framework and constrained by regularization terms.

7 CONCLUSION AND FUTURE WORK

This work investigated the spatio-temporal (ST) prediction problem from a multi-factor lens. We proposed a decomposed prediction strategy to address this problem theoretically. On top of that, we instantiated a novel ST

graph decomposition learning framework called STGDL. It consists of two components: an automatic graph decomposition module and a decomposed learning network. The former decomposes the original graph structure into several subgraphs corresponding to different latent factors, while the latter learns the partial ST data on each subgraph separately and integrates them for the final prediction. Extensive experiments on four datasets showed that deep ST models integrating with our framework can achieve significantly better performance. Empirical studies confirmed the advantages of STGDL on the effectiveness and interpretability. In the future, we plan to allow STGDL to learn human-understandable ST data patterns by bringing in expert knowledge.

ACKNOWLEDGMENTS

Jingyuan Wang acknowledges support from the National Natural Science Foundation of China (No. 7222022, 72171013, 72242101).

REFERENCES

- [1] L. Wang, D. Chai, X. Liu, L. Chen, and K. Chen, "Exploring the generalizability of spatio-temporal traffic prediction: Meta-modeling and an analytic framework," *IEEE Transactions on Knowledge and Data Engineering*, vol. 35, no. 4, pp. 3870–3884, 2023.
- [2] P. Xie, M. Ma, T. Li, S. Ji, S. Du, Z. Yu, and J. Zhang, "Spatio-temporal dynamic graph relation learning for urban metro flow prediction," *IEEE Transactions on Knowledge and Data Engineering*, vol. 35, no. 10, pp. 9973–9984, 2023.
- [3] Z. Pan, W. Zhang, Y. Liang, W. Zhang, Y. Yu, J. Zhang, and Y. Zheng, "Spatio-temporal meta learning for urban traffic prediction," *IEEE Transactions on Knowledge and Data Engineering*, vol. 34, no. 3, pp. 1462–1476, 2022.
- [4] S. Guo, Y. Lin, H. Wan, X. Li, and G. Cong, "Learning dynamics and heterogeneity of spatial-temporal graph data for traffic forecasting," *IEEE Transactions on Knowledge and Data Engineering*, vol. 34, no. 11, pp. 5415–5428, 2021.
- [5] C. Zhang, K. Zhao, and M. Chen, "Beyond the limits of predictability in human mobility prediction: context-transition predictability," *IEEE Transactions on Knowledge and Data Engineering*, vol. 35, no. 5, pp. 4514–4526, 2022.
- [6] J. Ji, J. Wang, J. Wu, B. Han, J. Zhang, and Y. Zheng, "Precision CityShield against hazardous chemicals threats via location mining and self-supervised learning," in *Proceedings of the 28th ACM SIGKDD Conference on Knowledge Discovery and Data Mining*, 2022, pp. 3072–3080.
- [7] Y. Li and Y. Zheng, "Citywide bike usage prediction in a bike-sharing system," *IEEE Transactions on Knowledge and Data Engineering*, vol. 32, no. 6, pp. 1079–1091, 2019.
- [8] J. Gu, Q. Zhou, J. Yang, Y. Liu, F. Zhuang, Y. Zhao, and H. Xiong, "Exploiting interpretable patterns for flow prediction in dockless bike sharing systems," *IEEE Transactions on Knowledge and Data Engineering*, vol. 34, no. 2, pp. 640–652, 2020.
- [9] J. Wang, Q. Gu, J. Wu, G. Liu, and Z. Xiong, "Traffic speed prediction and congestion source exploration: A deep learning method," in *2016 IEEE International Conference on Data Mining (ICDM)*, 2016.
- [10] J. Ji, J. Wang, Z. Jiang, J. Jiang, and H. Zhang, "STDEN: towards physics-guided neural networks for traffic flow prediction," in *Proc. of AAAI*, 2022, pp. 4048–4056.
- [11] J. Zhang, Y. Zheng, and D. Qi, "Deep spatio-temporal residual networks for citywide crowd flows prediction," in *Proc. of AAAI*, 2017, pp. 1655–1661.
- [12] S. Guo, Y. Lin, N. Feng, C. Song, and H. Wan, "Attention based spatial-temporal graph convolutional networks for traffic flow forecasting," in *Proc. of AAAI*, 2019, pp. 922–929.
- [13] D. Yang, K. Chen, M. Yang, and X. Zhao, "Urban rail transit passenger flow forecast based on lstm with enhanced long-term features," *IET Intelligent Transport Systems*, 2019.
- [14] Y. Li, R. Yu, C. Shahabi, and Y. Liu, "Diffusion convolutional recurrent neural network: Data-driven traffic forecasting," in *Proc. of ICLR*, 2018.
- [15] Z. Wu, S. Pan, G. Long, J. Jiang, and C. Zhang, "Graph wavenet for deep spatial-temporal graph modeling," in *Proc. of IJCAI*, 2019, pp. 1907–1913.
- [16] J. Wang, J. Ji, Z. Jiang, and L. Sun, "Traffic flow prediction based on spatiotemporal potential energy fields," *IEEE Transactions on Knowledge and Data Engineering*, vol. 35, no. 9, pp. 9073–9087, 2023.
- [17] H. Yao, X. Tang, H. Wei, G. Zheng, and Z. Li, "Revisiting spatial-temporal similarity: A deep learning framework for traffic prediction," in *Proc. of AAAI*, 2019, pp. 5668–5675.
- [18] J. Ji, J. Wang, Z. Jiang, J. Ma, and H. Zhang, "Interpretable spatio-temporal deep learning model for traffic flow prediction based on potential energy fields," in *2020 IEEE International Conference on Data Mining (ICDM)*. IEEE, 2020, pp. 1076–1081.
- [19] L. Bai, L. Yao, C. Li, X. Wang, and C. Wang, "Adaptive graph convolutional recurrent network for traffic forecasting," in *Advances in Neural Information Processing Systems*, 2020.
- [20] B. Yu, H. Yin, and Z. Zhu, "Spatio-temporal graph convolutional networks: A deep learning framework for traffic forecasting," in *Proceedings of the Twenty-Seventh International Joint Conference on Artificial Intelligence, IJCAI 2018, July 13-19, 2018, Stockholm, Sweden*, J. Lang, Ed. ijcai.org, 2018, pp. 3634–3640.
- [21] J. Ji, J. Wang, C. Huang, J. Wu, B. Xu, Z. Wu, Z. Junbo, and Y. Zheng, "Spatio-temporal self-supervised learning for traffic flow prediction," *Proc. of AAAI*, vol. 37, no. 4, pp. 4356–4364, 2023.
- [22] L. Alessandretti, U. Aslak, and S. Lehmann, "The scales of human mobility," *Nature*, 2020.
- [23] J. Wang, J. Wu, Z. Wang, F. Gao, and Z. Xiong, "Understanding urban dynamics via context-aware tensor factorization with neighboring regularization," *IEEE Transactions on Knowledge and Data Engineering*, 2019.
- [24] J. Wang, F. Gao, P. Cui, C. Li, and Z. Xiong, "Discovering urban spatio-temporal structure from time-evolving traffic networks," in *Web Technologies and Applications: 16th Asia-Pacific Web Conference, APWeb 2014, Changsha, China, September 5-7, 2014. Proceedings 16*. Springer, 2014, pp. 93–104.
- [25] Z. Fan, X. Song, and R. Shibasaki, "Cityspectrum: A non-negative tensor factorization approach," in *ACM UbiComp*, 2014, pp. 213–223.
- [26] X. Wang, P. Cui, J. Wang, J. Pei, W. Zhu, and S. Yang, "Community preserving network embedding," in *Proceedings of the AAAI conference on artificial intelligence*, vol. 31, no. 1, 2017.
- [27] C. Song, Z. Qu, N. Blumm, and A.-L. Barabási, "Limits of predictability in human mobility," *Science*, 2010.
- [28] J. Wang, Y. Mao, J. Li, Z. Xiong, and W.-X. Wang, "Predictability of road traffic and congestion in urban areas," *PloS one*, vol. 10, no. 4, p. e0121825, 2015.
- [29] T. M. Cover and J. A. Thomas, *Elements of Information Theory*. Wiley-Interscience, 2006.
- [30] A. Brabazon and M. O'Neill, *Natural Computing in Computational Finance*. Springer, 2008.
- [31] C. Xie, L. Yan, W. Li, and Z. Zhang, "Distributed power-law graph computing: Theoretical and empirical analysis," in *Advances in Neural Information Processing Systems*, 2014, pp. 1673–1681.
- [32] A. Y. Ng, M. I. Jordan, and Y. Weiss, "On spectral clustering: Analysis and an algorithm," in *Advances in Neural Information Processing Systems*. MIT Press, 2001, pp. 849–856.
- [33] C. Chen, K. Petty, A. Skabardonis, P. Varaiya, and Z. Jia, "Freeway performance measurement system: mining loop detector data," *Transportation Research Record*, 2001.
- [34] Z. Wu, S. Pan, G. Long, J. Jiang, X. Chang, and C. Zhang, "Connecting the dots: Multivariate time series forecasting with graph neural networks," in *Proceedings of the 26th ACM SIGKDD Conference on Knowledge Discovery and Data Mining*, 2020, pp. 753–763.
- [35] D. Liu, J. Wang, S. Shang, and P. Han, "MSDR: Multi-step dependency relation networks for spatial temporal forecasting," in *Proceedings of the 28th ACM SIGKDD Conference on Knowledge Discovery and Data Mining*, 2022, pp. 1042–1050.
- [36] J. Wang, J. Jiang, W. Jiang, C. Li, and W. X. Zhao, "LibCity: An open library for traffic prediction," in *Proceedings of the 29th International Conference on Advances in Geographic Information Systems*, 2021.
- [37] A. Buluç, H. Meyerhenke, I. Safro, P. Sanders, and C. Schulz, *Recent advances in graph partitioning*. Springer, 2016.
- [38] A. E. Feldmann and L. Foschini, "Balanced partitions of trees and applications," *Algorithmica*, vol. 71, no. 2, pp. 354–376, 2015.

- [39] J. Wang, H. Shi, J. Ji, X. Lin, and H. Tian, "High-resolution data on human behavior for effective covid-19 policy-making—wuhan city, hubei province, china, january 1–february 29, 2020," *China CDC Weekly*, vol. 5, no. 4, pp. 76–81, 2023.
- [40] Y. Zheng, *Urban computing*. MIT Press, 2019.
- [41] J. Wang, C. Chen, J. Wu, and Z. Xiong, "No longer sleeping with a bomb: A duet system for protecting urban safety from dangerous goods," in *Proceedings of the 23rd ACM SIGKDD International Conference on Knowledge Discovery and Data Mining*. ACM, 2017, pp. 1673–1681.
- [42] X. Zhang, C. Huang, Y. Xu, L. Xia, P. Dai, L. Bo, J. Zhang, and Y. Zheng, "Traffic flow forecasting with spatial-temporal graph diffusion network," in *Proc. of AAAI*, 2021, pp. 15 008–15 015.
- [43] C. Zheng, X. Fan, C. Wang, and J. Qi, "GMAN: A graph multi-attention network for traffic prediction," in *Proc. of AAAI*, 2020, pp. 1234–1241.
- [44] G. Karypis and V. Kumar, "Multilevel k-way hypergraph partitioning," in *Proceedings of the 36th annual ACM/IEEE design automation conference*, 1999, pp. 343–348.
- [45] R. Andersen, F. Chung, and K. Lang, "Local graph partitioning using pagerank vectors," in *2006 47th Annual IEEE Symposium on Foundations of Computer Science (FOCS'06)*, 2006.
- [46] T. Kawamoto, M. Tsubaki, and T. Obuchi, "Mean-field theory of graph neural networks in graph partitioning," in *Advances in Neural Information Processing Systems*, 2018, pp. 4366–4376.
- [47] A. Nazi, W. Hang, A. Goldie, S. Ravi, and A. Mirhoseini, "GAP: Generalizable approximate graph partitioning framework," *ArXiv preprint*, vol. abs/1903.00614, 2019.
- [48] T. Mallick, P. Balaprakash, E. Rask, and J. Macfarlane, "Graph-partitioning-based diffusion convolutional recurrent neural network for large-scale traffic forecasting," *Transportation Research Record*, vol. 2674, no. 9, pp. 473–488, 2020.

Jiahao Ji is a Ph.D. candidate at the School of Computer Science and Engineering, Beihang University. He received his B.S from Beihang University in 2019. His research interests include spatio-temporal data mining, interpretable machine learning, and urban computing.



Jingyuan Wang received the Ph.D. degree from the Department of Computer Science and Technology, Tsinghua University. He is currently a Professor at School of Computer Science and Engineering, Beihang University. He is also the head of the Beihang Interest Group on SmartCity (BIGSCity), and Vice Director of the Beijing City Lab (BCL). His general area of research is data mining and machine learning, with special interests in smart cities and spatiotemporal data analytics.



Yu Mou is a graduate student at the School of Computer Science and Engineering, Beihang University. He received his B.S. from Beihang University in 2022. His research interests include road representation learning and spatio-temporal data mining.



Cheng Long is currently an Assistant Professor at the School of Computer Science and Engineering, Nanyang Technological University. He received his Ph.D. degree from the Hong Kong University of Science and Technology, Hong Kong, in 2015, and his BEng degree from South China University of Technology, China, in 2010. His research interests are broadly in data management and data mining.



APPENDIX A

A.1 Proof of Lemma 1

Proof: According to the graph decomposition step, it decomposes the original traffic graph G into K subgraphs, namely $\{G_k\}_{k=1}^K$. Consequently, the original ST prediction problem P defined on G is divided into K subproblems, namely $\{P_k\}_{k=1}^K$. Each subproblem aims to predict the future ST data $\mathbf{X}_k^{(t+1)}$ corresponding to G_k . Before delving into further proof, we give two necessary definitions.

Definition 2 (Problem Scale). *Given a prediction problem P on ST graph data $\mathcal{G}^{(t-T:t)} = (G, \mathbf{X}^{(t-T:t)})$ with graph structure $G = (\mathcal{V}, \mathcal{E}, \mathbf{A})$, we define the problem scale B_P as the number of graph nodes, i.e., $B_P = |\mathcal{V}|$.*

Definition 3 (Problem Independence). *Given two ST prediction problems P_1 and P_2 , they are independent ($P_1 \perp P_2$) if and only if graph edge sets \mathcal{E}_1 and \mathcal{E}_2 of both problems are orthogonal, i.e., $\mathcal{E}_1 \cap \mathcal{E}_2 = \emptyset$.*

For any subproblem $P_k, k \in [1, K]$, we know $G_k \subset G$, that is $|\mathcal{V}_k| < |\mathcal{V}|$. Thus, we can have $B_{P_k} < B_P$, meaning the scale of every subproblem is *smaller* than that of the original problem. On the other hand, the subgraphs satisfy $\bigcap \mathcal{E}_k = \emptyset$, so each pair of graph edge sets satisfy

$$\forall j, k \in [1, K], \mathcal{E}_j \cap \mathcal{E}_k = \emptyset \Rightarrow P_j \perp P_k. \quad (13)$$

This means that any two subproblems are *independent*. \square

A.2 Proof of Lemma 2

Proof: According to Thm. 2, we know that $\forall k \in [1, K], e_k < e$. Here, e_k is the error rate lower bound of solving the k -th subproblem P_k , while e is that of directly solving the original problem P . From the data generation perspective, the partial ST data relevant to the k -th subproblem can be considered as samples of a random variable X_k . We use σ_k^2 to denote the variance of X_k . Then, we analyze the prediction error lower bound of the k -th subproblem, namely $ELBO_k$. The error comes from two cases: *i*) predictions are correct and *ii*) predictions are incorrect. Thus, the $ELBO_k$ can be computed by the expectation of errors in both cases:

$$ELBO_k = e_k \cdot r_k^0 + (1 - e_k) \cdot r_k^1. \quad (14)$$

where e_k is the error rate lower bound indicating the minimal probability of making incorrect predictions, and r_k^0 is the error expectation when the predictions are incorrect. r_k^1 is that when the predictions are correct.

We know $r_k^1 = 0$. As for r_k^0 , it can be calculated by the error between every possible prediction and ground truth:

$$r_k^0 = \sum_i p_i^{(k)} \sum_j p_j^{(k)} (x_j^{(k)} - x_i^{(k)})^2, \quad (15)$$

where $x_i^{(k)}$ is a ground truth with probability $p_i^{(k)}$, and $x_j^{(k)}$ is a prediction with probability $p_j^{(k)}$. Solving Eq. (15) is equivalent to finding the solution of $\mathbb{E}[(X - Y)^2]$ with constraint *i*) $X \perp Y$ and *ii*) variables X, Y are the instance of the same random variable. Since

$$\begin{aligned} \mathbb{E}[(X - Y)^2] &= \mathbb{E}[X^2 - 2XY + Y^2] \\ &= \mathbb{E}[X^2] - 2\mathbb{E}[XY] + \mathbb{E}[Y^2] \\ &= \mathbb{E}[X^2] - 2\mathbb{E}[X]\mathbb{E}[Y] + \mathbb{E}[Y^2], \end{aligned} \quad (16)$$

we substitute X, Y with a unified variable Z and have

$$\begin{aligned}\mathbb{E}[(X - Y)^2] &= \mathbb{E}[Z^2] - 2\mathbb{E}[Z]\mathbb{E}[Z] + \mathbb{E}[Z^2] \\ &= 2(\mathbb{E}[Z^2] - \mathbb{E}^2[Z]) = 2D(Z),\end{aligned}\quad (17)$$

where $D(Z)$ is the variance of random variable Z . Through the above derivations, we know that $r_k^0 = 2\sigma_k^2$. Taking r_k^1 and r_k^0 into Eq. (14), we can have

$$ELBO_k = e_k \cdot 2\sigma_k^2 + (1 - e_k) \cdot 0 = 2e_k\sigma_k^2. \quad (18)$$

That is, the error lower bound of the k -th subproblem is $2e_k\sigma_k^2$. \square

A.3 Proof of Lemma 3

Proof: By combining the solutions to all subproblems, we can have an integrated solution for the original problem. From Lemma 1, the subproblems are independent of each other. This means that the covariance of any two subproblems is zero, thereby making the covariance of the relevant random variables zero. Therefore, the error lower bound of the combined solution (E_d) can be computed by the summation of lower bounds of all subproblems, i.e., $E_d = \sum_{k=1}^K ELBO_k = \sum_{k=1}^K 2e_k\sigma_k^2$. \square

APPENDIX B

B.1 Proof of Error Rate Lower Bound

Theorem 2. *In the decomposed prediction strategy, the error rate lower bound of any subproblem (e_k) is smaller than that of the original problem (e), i.e., $\forall k \in [1, K], e_k < e$.*

Here, the error rate lower bound (e) describes the minimal probability of making incorrect predictions. It can be computed by the predictability upper bound (π^{max}) [27] via

$$e = 1 - \pi^{max}. \quad (19)$$

Predictability refers to the extent to which future data can be accurately predicted with only past observations. The data to be predicted in this paper are ST data. They are naturally time series, allowing us to use tools from information theory, including entropy [30] and Fano's inequality [29], to measure the predictability. Next, we prove Thm. 2 through predictability and information entropy.

Proof: According to Fano's inequality [29], we can compute the predictability upper bound (π^{max}) by solving

$$\begin{aligned}S &= H(\pi^{max}) + (1 - \pi^{max}) \log(M - 1) \\ &= -\pi^{max} \log(\pi^{max}) - (1 - \pi^{max}) \log(1 - \pi^{max}) \\ &\quad + (1 - \pi^{max}) \log(M - 1).\end{aligned}\quad (20)$$

Here, S is the entropy of data distribution. $H(\pi^{max})$ is the entropy of π^{max} . M is the data state number, and it will be fixed once the data is given.

We treat S as a function π^{max} . Taking the first-order derivation of S over π^{max} yields

$$S' = -\log(\pi^{max}) + \log(1 - \pi^{max}) - \log(M - 1). \quad (21)$$

Then, taking the second-order derivation of S yields

$$S'' = \frac{1}{\pi^{max}(1 - \pi^{max})}. \quad (22)$$

Since $\pi^{max} \in [0, 1]$, the inequality $S'' < 0$ always holds. This indicates that S is a concave function on π^{max} and S has a maximum value.

Let $S' = 0$ to obtain the maximum value point as $\pi^{max} = 1/M$. That is, when $\pi^{max} > 1/M$, S is a monotonically decreasing function of π^{max} . Oppositely, when $\pi^{max} < 1/M$, S is a monotonically increasing function of π^{max} . Since it was found that $\pi^{max} > 1/M$ usually holds for ST data such as human mobility data [27], [28], S can generally be considered as a monotonically decreasing function of π^{max} . This means that the larger S is, the smaller the corresponding π^{max} is.

Next, it is sufficient to compare entropy(S) corresponding to the subproblems and the original problem to obtain a relation for predictability upper bound (π^{max}), and thus for the error rate lower bound (e). To this end, we introduce the following lemma.

Lemma 4. *The entropy of ST data distribution under any single factor (S_k) is smaller than that under multiple factors (S), i.e., $\forall k \in [1, K], S_k < S$.*

According to Lemma 4, $S_k < S$ holds for any k . Since S monotonically decrease with π^{max} , we have $\pi_k^{max} > \pi^{max}$ for any k . Bringing the inequality into Eq. (19), we have $\forall k \in [1, K], e_k < e$. \square

B.2 Proof of Lemma 4

Proof: Before delving into the proof, we clarify some terms. We use X_k ($k \in [1, K]$) to denote the random variable relevant to ST data under the k -th factor. S_k is the corresponding entropy. Since the data under multiple factors is a mixture of data under all single factors, S is the joint entropy of all random variables and can be defined as

$$S = H(X_1, X_2, \dots, X_K) = \sum_{k=1}^K H(X_k | X_{k-1}, \dots, X_1), \quad (23)$$

where $H(X_k | X_{k-1}, \dots, X_1)$ is the conditional entropy.

There are two steps to prove this lemma: *i*) proving $S_1 < S$. *ii*) extending the conclusion of S_1 to S_k . For step *i*), we expand the summation term in Eq. (23):

$$\begin{aligned}S &= H(X_1, X_2, \dots, X_K) \\ &= H(X_1) + H(X_2 | X_1) + \dots + H(X_K | X_{K-1}, \dots, X_1) \\ &\geq H(X_1) = S_1.\end{aligned}\quad (24)$$

The last step is derived from the non-negativity of conditional entropy. It means that in step *ii*), each term after $H(X_1)$, such as $H(X_2 | X_1)$, is non-negative.

For step *ii*), according to the symmetry of entropy, entropy should be unchanged if the outcomes X_k are re-ordered. Therefore, we can rewrite the expression of S as

$$S = (X_k, X_1, \dots, X_{k-1}, X_{k+1}, \dots, X_K). \quad (25)$$

Here, we adjust X_k from the k -th position to the first position. This operation does not change the value of entropy. By using the rules of Eq. (24), we can obtain

$$S_k \leq S, k \in [1, K]. \quad (26)$$

The equal sign is obtained when ST data of all factors are the same. This is nearly impossible in real-world scenarios, so we remove the equal sign and reach the final conclusion that $\forall k \in [1, K], S_k < S$. \square